2018-01-1287 Published 03 Apr 2018

Exhaust and Muffler Aeroacoustics Predictions using Lattice Boltzmann Method

Clément Nardari EXA GmbH

Adrien Mann Exa Corporation

Tobias Schindele Faurecia

Citation: Nardari, C., Mann, A., and Schindele, T., "Exhaust and Muffler Aeroacoustics Predictions using Lattice Boltzmann Method," SAE Technical Paper 2018-01-1287, 2018, doi:10.4271/2018-01-1287.

Abstract

Exhaust systems are a necessary solution to reduce combustion engine noise originating from flow fluctuations released at each firing cycle. However, exhaust systems also generate a back pressure detrimental for the engine efficiency. This back pressure must be controlled to guarantee optimal operating conditions for the engine. To satisfy both optimal operating conditions and optimal noise levels, the internal design of exhaust systems has become complex, often leading to the emergence of undesired noise generated by turbulent flow circulating inside a muffler. Associated details needed for the manufacturing process, such as brackets for the connection between parts, can interact with the flow, generating additional flow noise or whistles.

To minimize the risks of undesirable noise, multiple exhaust designs must be assessed early to prevent the late detection of issues, when design and manufacturing process are frozen. However, designing via an experimental approach is challenging. Since the construction process does not exist yet, physical prototypes lack the details associated to manufacturing. In addition, experimental optimization is time-consuming, as each design iteration will require a new physical prototype, thus increasing costs and development times, or limiting the explored design space.

Alternatively, larger design spaces may be explored using virtual optimization, while removing the limitations of physical testing. Exhaust flow and acoustic simulations with the Lattice-Boltzmann Method (LBM) have been shown accurate as well as feasible within the product design cycle timing. Using noise sources detection techniques, such as Flow-Induced Noise Detection (FIND), understanding the noise generation mechanism associated to the optimal designs is also possible to orient future design decisions. In this study, after validating the ability of the approach at capturing flow noise and whistles, a characterization of the bracket design connecting tailpipe and muffler is performed to minimize the risk of whistle in the final product.

Introduction

Combustion engines are a source of noise by design since the generated rotational energy comes from a combustion process associated to high levels of pressure fluctuations. To reduce the acoustic drawback of the combustion engine, the industry has developed exhaust systems. Exhaust systems are composed of pipes, heat shields, mufflers, perforated baffles, acoustic wool, elbows, valves, water management canals, tail finishers and so forth. By combining such exhaust systems with combustion engines, it is possible to reduce the noise generated by the engine and consequently meet all noise regulations. However, the benefit of using an exhaust system is not without drawbacks. One of these drawbacks is associated to the connection between parts of the system. These connections tend to be production time bottlenecks on an assembly line. Moreover, these connections must be robust and last the complete life-cycle of the car, the bus or the off-highway machine employing the exhaust system. To reduce assembly time while ensuring durability, exhaust manufacturers have come up with a novel joining technology. This technology is cheaper and faster but it creates a forward-facing edge.

Among Computational Fluid Dynamics (CFD)/ Computational AeroAcoustics (CAA) methods, Lattice Boltzmann based Methods (LBM) have showed in previous studies focusing on exhaust system flow induced noise their ability to predict noise levels accurately [1, 2, 3]. These methods can both accurately predict broad banded noise phenomena [4] as well as narrow banded behaviors such as whistling and resonances [5, 6].

The purpose of this project is to understand the impact of this geometrical feature on the overall flow noise of the complete system. Therefore, this paper will first validate the simulation method. Then provide an analysis of the noise mechanism near the joining protuberance. Finally, it will give insight if this novel joining technology can be used while avoiding a whistling pattern.

Experiment

In this project, the measurements are conducted in a fully anechoic room. The silencer is plugged to a cold blower by a metallic inlet pipe with an inlet mass flow of 850 kg.h^{-1} at 20°C. The ambient conditions are 960 mbar and 20°C.

Figure 1 shows the test environment. As it is a fully anechoic chamber, the walls are covered with radiation absorber materials to minimize the noise reflections in the chamber. A wire mesh is there to make the work of the test engineer possible without any effects on wave propagation.

Two microphones are recording the pressure fluctuations. These two probes record the near-field, 500 mm away from the muffler exit at 45° from the jet flow axis.

The green arrows in Figure 2 point out the joining edge location and shape. This geometrical protuberance is composed of a sharp rounded edge and a closed cavity following the edge. The blue arrow is giving the flow stream direction. Thus, the joining edge is forward facing the flow.

FIGURE 1 Test rig

FIGURE 2 Joining edge prototype X-Ray picture

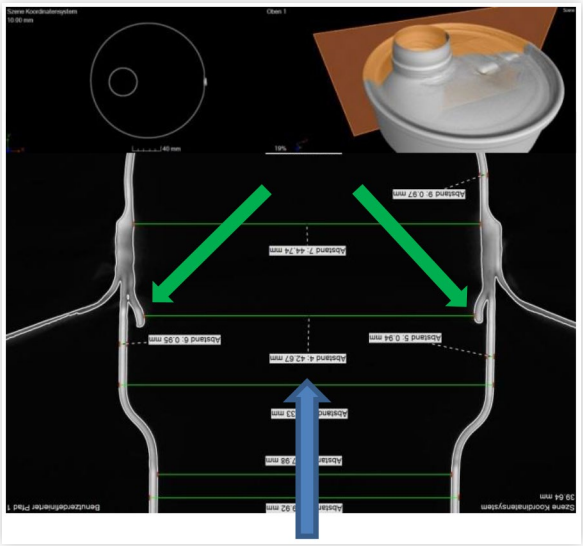

Numerical Details

Approach

Flow noise simulations for the muffler system in this paper were performed using the PowerFLOW 5.3 commercial CFD solver. The CFD/CAA solver PowerFLOW 5.3 based on the Lattice Boltzmann Method is used to calculate unsteady flow physics and the corresponding flow-induced noise generation and radiation. Lattice-based methods are by nature explicit, transient and compressible. They are an alternative to traditional CFD methods based on the discretization of the Navier-Stokes equations and derived variations [7, 8, 9, 10, 11, 12]. The basic idea of LBM is to track the advection and collisions of fluid particles. Since the average number of particles in a representative volume of fluid far exceeds the computing power required to track them individually, the particles are grouped into an integer number of discrete directions with index i. The computation follows the particle distribution function f_i which represents the number of particles per unit of volume, also called voxel, at a specific time and location moving with velocity c_i. As in statistical physics, the flow variables such as density and velocity are determined by taking the appropriate moments, i.e. summations over the set of discrete directions, of the particle distribution function [13, 14, 15, 16, 17, 18, 19, 20, 21, 21]. Recent improvements in modeling the temperature scalar equation have further enhanced the accuracy of the temperature calculations in the flow solver [22]. LBM is used and validated across many aeroacoustics applications such as automotive wind-noise [23,24], HVAC system noise [25,26], acoustic propagation [27,28], airframe noise [29,30], sunroof buffeting [31] and exhaust systems noise [1, 2, 3, 4, 5, 6]. Further details on LBM can be found in the cited references.

An initial characterization is conducted using Latin Hypercube sampling [32], which provides a random, uniform sampling of PowerFLOW simulations throughout the design space. A Kriging [33] response surface model (RSM) approximates the relationship between the input and output variables of the study, interpolating the performance data. A series of charts based on the RSM provides detailed insight into the design trends, such as local and global sensitivities and performance trade-offs. The accuracy of the RSM is iteratively refined and validated using additional batches of PowerFLOW simulations, targeting sampling regions with higher error and/or optimal performance. More details are described in [34].

Model

All the geometrical details of the prototype are maintained in the simulation model, and no simplifications have been made to ensure accuracy of the predictions.

Figure 3 shows the simulated model geometry which is point by point similar with the prototype tested. The inlet of the muffler is extended in the up-stream direction and a sponge zone approach is used to damp all acoustic waves travelling back the inlet pipe. These muffler´s characteristics are standard; it is made from 1 mm thick metal sheet, 3.5 mm perforated baffles, acoustic wool and a tulip at the outlet manifold.

The mean upstream mass flow is imposed on the extended inlet at 850 kg.h^{-1} and 25°C. The computational domain is

FIGURE 3 Simulated model

FIGURE 4 Joining edge simulation model

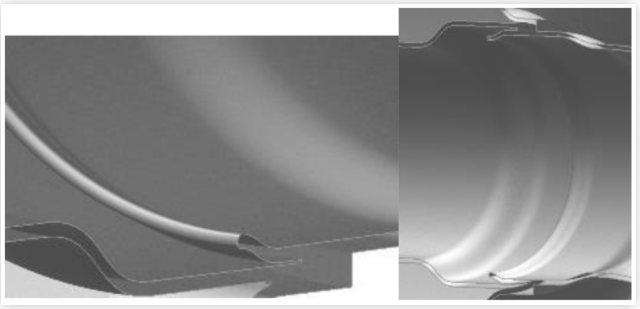

subdivided into numerous variable resolution volumes. The purpose of these resolution volumes is to tailor the grid as needed to resolve the flow structures. The computational volume is bounded by solid walls with pressure outlet boundary condition set to P=1013 hPa. A sponge zone strategy is also used to prevent reflections of acoustic waves on the simulation volume boundaries. Simulated physical time is 0.2 second and initialized with the flow from a coarser simulation. To reach convergence of the main flow features faster, the simulation is divided into two simulations: the coarse and the fine simulation. The coarse simulation has a bigger smallest voxel size and thus allows for greatly reduced simulation times to capture mesoscopic flow behavior. The coarse run is not used to generate any measurement files, only as a seed file for the fine simulation.

Before post processing the simulation, a convergence study has been performed to know at what time all physical values are converged. It was determined that 0.1 second of simulation time is enough to achieve this convergence. Therefore, the SPL plots and the dB maps showed later in this study are using the physical quantities measured from 0.1 second to 0.2 second.

Baseline Results and Correlation

SPL

Experiments and simulation are shown together in Figure 5. Broadband content is captured within 3 dB(A) over all frequencies. Three significant peaks are captured at 4100 Hz,

FIGURE 5 Sound Pressure Level 32 Hz band A-Weighted Decibel

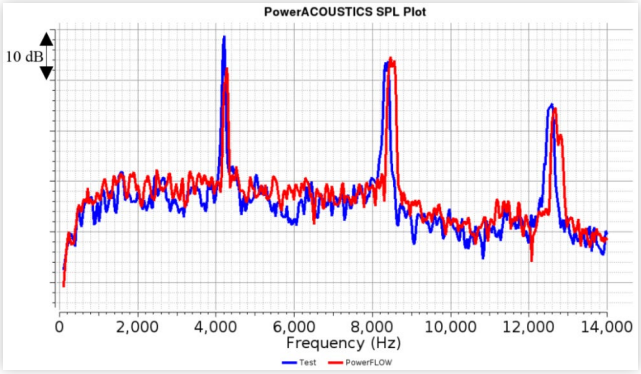

8200 Hz and 12300 Hz. The second and the third peaks are captured within 1 dB(A) while the first peak is captured within 4 dB(A). The slight shift in frequency and in amplitude of the peaks can be explained by production tolerances between the Computer-Aided Design (CAD) model and the prototype. A variation of the mass flow is another possible explanation.

The overall sound pressure level over [100,14000] Hz is captured within less than 1dB(A)

Flow Noise Analysis

Flow structures, also called vortices, are present in turbulent flows and generate noise through their dynamics. Vortex dynamics is not only vortex motion, but also vortex deformation induced by the interactions with the flow or a surface. Pressure fluctuations observed in a flow can be acoustic waves, or the result of turbulent high vorticity behavior. Pressure oscillations from the latter, often associated to hydrodynamic effects, typically carry much more energy content, and lead to higher levels of pressure fluctuations. Acoustic pressure fluctuations are moving at the speed of sound whereas, pressure oscillations due to fluid structures are convected at a speed close to the mean flow velocity.

Figure 6 shows a close-up view of the instantaneous time derivative of pressure with filled contours of the quantity. This is a slice along the outlet pipe centreline. In this figure, acoustic waves are visible in the muffler, in the pipes and outside. Time derivative of pressure tends to emphasize the acoustic pressure fluctuations, specifically at higher frequencies, providing a

FIGURE 6 Pressure time derivative snapshot

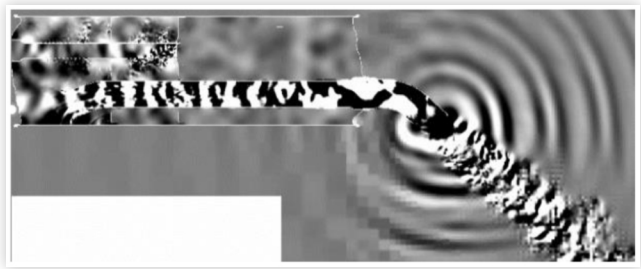

relevant picture of the acoustic field. Pressure fluctuations of acoustic nature, propagate at the speed of sound while pressure fluctuations of hydrodynamic nature, associated to vortices generated by the flow, are transported and travel at a speed close to the local flow speed. Acoustic waves travelling in the outlet pipe are observed in Figure 6. Since the waves are traveling upstream and downstream, the acoustic source is potentially associated to the joining edge.

dBmaps, visualize local pressure fluctuation amplitudes over a defined frequency band. The two pictures of Figure 7 show the first orthogonal mode of the outlet tail pipe and the first harmonic of this mode.

A band pass filter snapshot, shows pressure oscillations within a specific frequency band. It contains both acoustics and hydrodynamic fluctuations, as visible in Figure 8, where:

- Blue is low pressure iso-surfaces: below -150 dimless
- Red is high pressure iso-surfaces: above 150 dimless

This measurement shows in 3-Dimension the wave propagation of the resonance. The origin of acoustics is primarily a radial pipe mode next to the joining edge with then propagation of the acoustic waves through the pipe in both directions as plane waves. Moreover, this snapshot shows that no pressure fluctuations with such a high amplitude are visible at this frequency inside the muffler. Thus, the muffler is potentially damping these acoustic waves.

Vorticity magnitude is used to identify turbulent/non-uniform areas and λ_2 iso-surfaces colored by vorticity magnitude are used to identify the vortices. If there are vortices, there could be associated to noise source. This quantity thus enables the visualization of potential noise-generating flow structures.

FIGURE 7 dBmaps 12th octave band

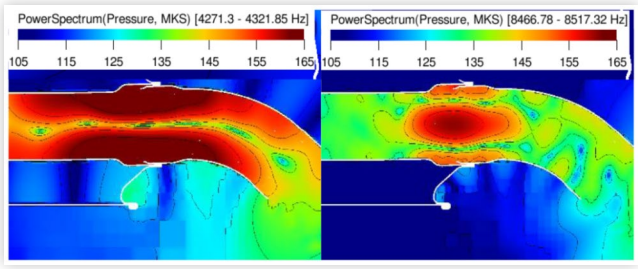

FIGURE 8 Volume pressure band pass filter [4200,4400] Hz

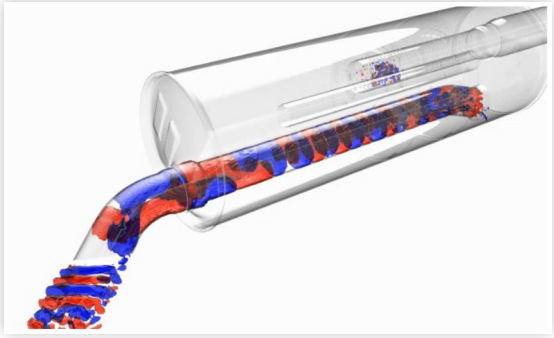

From the two snapshots in Figures 9 and 10, a periodic vortex shedding is observed at the outlet pipe expansion. These vortices are transported toward the joining edge connecting the muffler outlet pipe with the outlet tail pipe. They are then chopped and trapped by this edge, generating periodic acoustic excitations at this location exciting the normal pipe mode of the outlet tail pipe.

Characterization

The goal of a characterization is to understand the behavior of a system in response to several parameters. Given the complexity of flow noise generation mechanisms, experimental or empirical methods fail in general to characterize such nonlinear phenomena. At a high level, the purpose of this characterization is to know when the resonance will occur and when it will not. Moreover, the goal is to understand what makes a design whistle and how to prevent this whistling from happening in the production part. Numerous of geometrical or non-geometrical parameters could be considered. From these parameters, two have been chosen:

- Characteristic length
- Mass flow

The characterization was split in two phases: the strategy of the first phase is to explore the influence of the mass flow

FIGURE 9 Vorticity magnitude

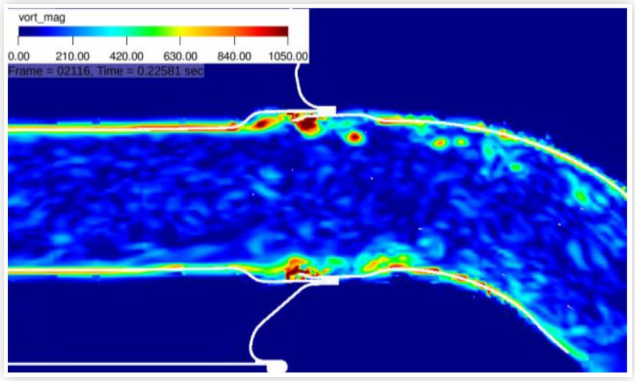

FIGURE 10 λ_2 iso-surfaces colored by vorticity magnitude

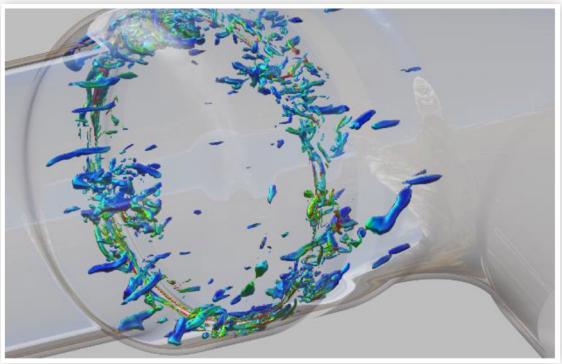

and determine when this phenomenon can arise. The second phase of the characterization considers the two parameters varying simultaneously. In both phases, the objective function of this characterization is the maximum SPL amplitude of the two resonance peaks.

The result of this characterization is a 3D-response surface. Because of the nonlinearity of the underlying aeroacoustics physics, numerous local extrema potentially exist in the goal design space. Consequently, a gradient-based method would not be able to find all the extrema, converging only to a single extremum.

Instead of running many simulations to define the response space, a Kriging algorithm has been used, allowing the user to accurately approximate a continuous response surface from a discrete database. It can model high nonlinearities in the response, needs fewer sampling points to be trained compared to higher-order polynomial models, and interpolates the sampling data, rather than just providing a best fit like regression functions. This is appropriate given the accuracy of the simulations performed.

Design of Experiment

As explained before, the input variables for the characterization are the mass flow and the edge axial distance. Three validation simulations have been run before: RUN 300, RUN 850, RUN 1000 and will be added to the data base to train the response surface. The design space of this characterization is:

- Mass flow ∈ [100,1000] $kg.h^{-1}$
- Edge axial distance ∈ [0,1]

The edge axial distance shown in figure 11 is a geometrical parameter. A morph is performed on the initial geometry to change this parameter. PowerDELTA has been used to execute the morphing function. 0 means initial position and 1 means the joining edge is touching the expansion of the outlet pipe.

To populate the design space, the Latin Hypercube sampling algorithm has been used.

Table 1 shows the run names, the edge axial distances, the first peak amplitudes, the second peak amplitudes and the goal function, that is the maximum of the first and the second peak amplitudes.

$$Goal = max(First, Second)$$

All the simulations have been run and Figure 12 shows the repartition of the runs within the design space colored by the amplitude of the goal function. The plot clearly shows that it is most likely to have a resonance with a mass flow greater than 600 $kg.h^{-1}$. However, there are two runs, Sweep 2 and DoE 3, with a mass flow of 781 $kg.h^{-1}$ that do not whistle.

FIGURE 11 Joining edge

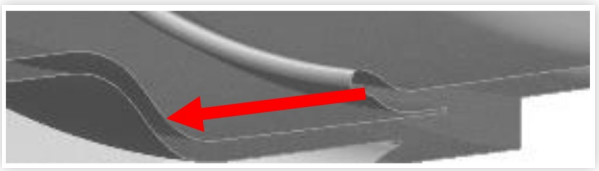

TABLE 2 Simulation input and output values

Case	Edge axial distance	Mass Flow (kg.h-1)	1st(dBA)	2sd(dBA)	Goal(dBA)
RUN 850	0	850	22.8	27.4	27.4
RUN 300	0	300	0	0	0
RUN 1000	0	1000	9.7	11.8	11.8
Sweep 1	0.84	988.9	0	27	27
Sweep 2	0.84	781	0	0	0
Sweep 3	0.84	619.3	0	0	0
Sweep 4	0.84	339.4	0	0	0
Sweep 5	0.84	692.6	0	8	8
Sweep 6	0.84	262.5	0	0	0
Sweep 7	0.84	153.9	0	0	0
Sweep 8	0.84	455.4	5.9	0	5.9
DoE 0	0.931	861.9	0	12.7	12.7
DoE 1	0.451	545.5	0	0	0
DoE 2	0.069	988.9	4.2	11.8	11.8
DoE 3	0.732	781	0	0	0
DoE 4	0.609	619.3	29.5	24.9	29.5
DoE 5	0.27	339.4	0	0	0
DoE 6	0.563	692.6	33.3	32.3	33.3
DoE 7	0.153	262.5	0	0	0
DoE 8	0.844	153.9	0	0	0
DoE 9	0.322	455.4	0	0	0

FIGURE 12 All the runs colored by the goal function

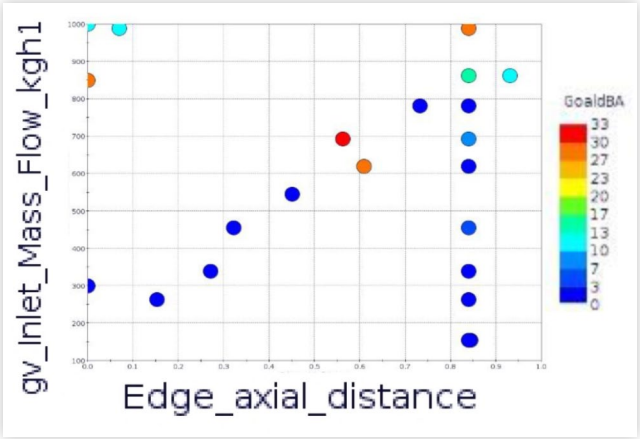

Response Surface

To go from the discrete world of the data base, to the continuous world of the surrogate model, the Kriging algorithm has been used to generate the response surface. This surface is a 3-D surface:

- X axis is the edge axial distance
- Y axis is the mass flow
- Z axis is Max(1^{st} peak, 2^{sd} peak)

The response surface shown in figure 13 needs more points to make the interpolation more accurate. A batch of six new simulations in the region: x ∈ [0.1,0.5] & y ∈ [600,1000]

and x ∈ [0.3, 0.8] & y ∈ [200, 500] would make the response more accurate.

Flow Noise Analysis

Following the design of experiment part, the two runs DoE 3 and DoE 6 will be analyzed further to understand why DoE 6 has the strongest resonance of all the runs and why DoE 3 that is slightly different than DoE 6 does not resonate. This analysis will be completed in the final version of this paper.

DoE 3 has a high mass flow and the joining edge is close to the expansion outlet. Therefore, due to the inertia of the flow, the vortices generated by the expansion of the outlet pipe are transported strait in the direction of the flow and avoid the joining edge.

FIGURE 13 Response surface

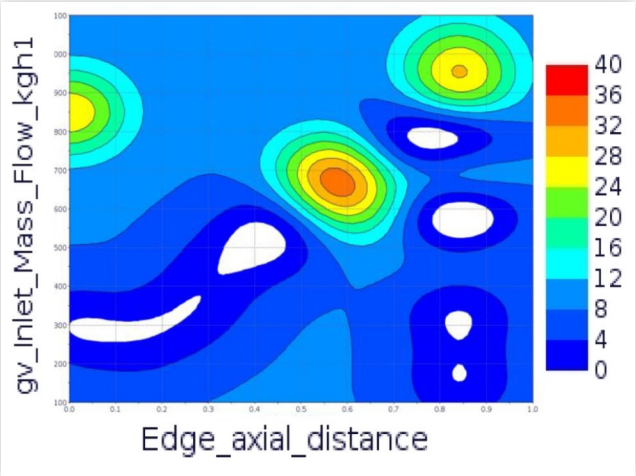

FIGURE 13 DoE 3 Velocity magnitude

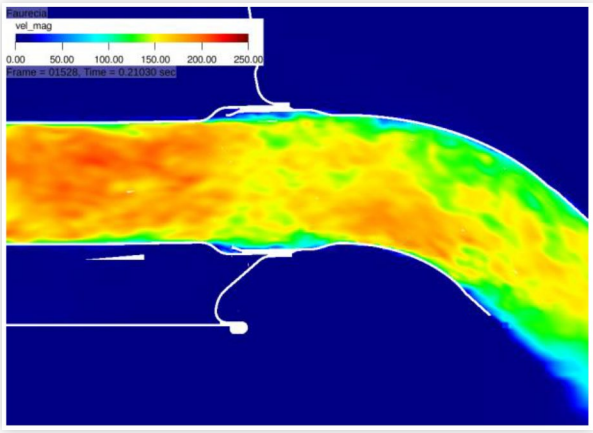

FIGURE 14 DoE 3 dBmaps 12th octave band

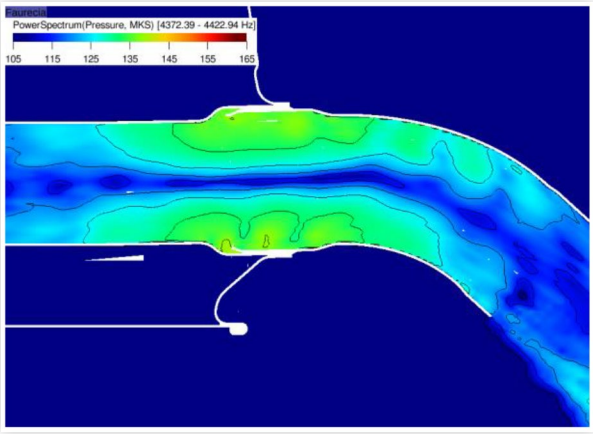

FIGURE 15 DoE dBmaps 12th octave band

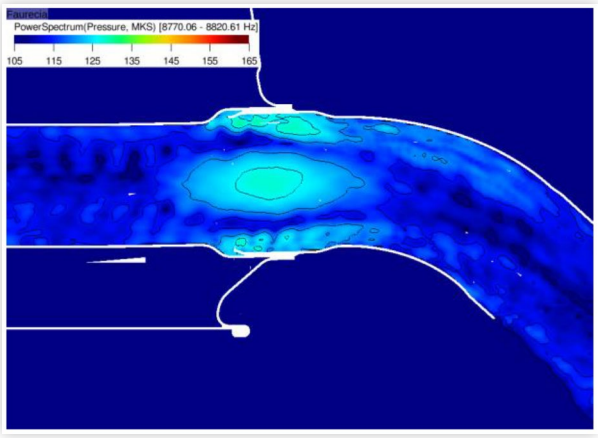

FIGURE 17 DoE 6 Velocity magnitude

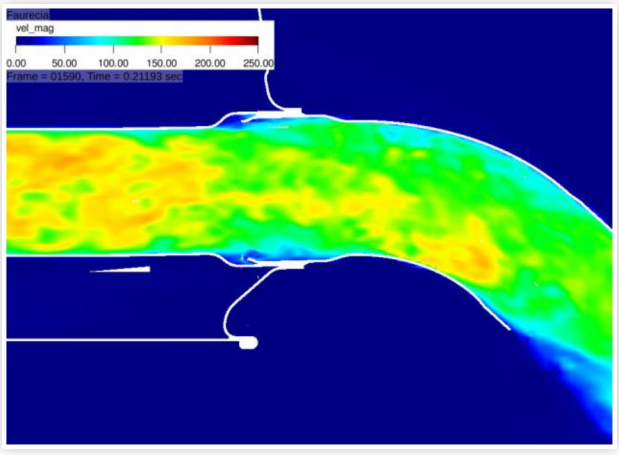

FIGURE 18 DoE 6 dBmaps 12th octave band

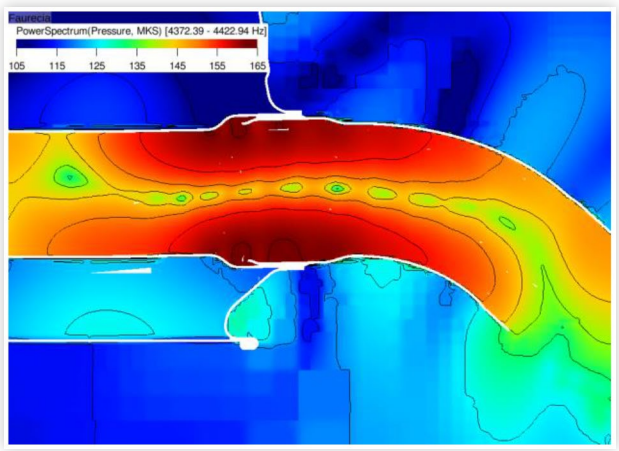

FIGURE 19 DoE 6 dBmaps 12th octave band

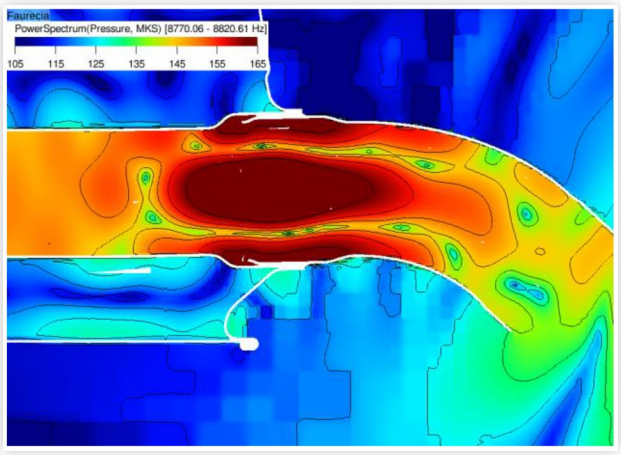

DoE 6 has a smaller mass flow than DoE 3 but the edge is further away from the expansion outlet. Therefore, the periodic vortex street is going right in the direction of the joining edge generating this significant resonance.

Conclusion

This project had three goals: validating the LBM simulation model, understanding the flow noise behavior of the joining edge and finding a usage envelope for the final product. The LBM model has been validated since the OASPL is captured within 0.7 dB(A) and the narrow-banded singularities within 4 dB(A). Thanks to the advanced post-processing performed, the noise mechanism has been understood: the outlet pipe expansion generates a periodic vortex shedding, the flow transports these vortices in the direction of the joining edge, they are sliced and stuck by this edge generating a periodic acoustic excitation and finally this excitation excites the normal pipe mode of the outlet pipe. The characterization has shown the noise mechanism of this system is highly non-linear. Moreover, below 500 kg.h-1, the resonance is not occurring. The next step of this project would be to plot the error of the Kriging process and add some more simulations where the error is high to improve the response surface.

References

1. Mann, A., Kim, M., Neuhierl, B., Perot, F., Powell, R., Tose, T. and Krueger, J., 2015, "Exhaust and Muffler Aeroacoustics Predictions using Lattice Boltzmann Method" [J], *SAE Int. J. Passeng. Cars - Mech. Syst.* 8(3):1009-1017, 2015, doi:10.4271/2015-01-2314.
2. Mann, A., Nair, R., Gill, J., Birschbach, B. et al., "Flow Noise Predictions for Single Cylinder Engine-Mounted Muffler Using a Lattice Boltzmann Based Method," *SAE Int. J. Engines* 10(4):2067-2076, 2017.
3. Mann, A., Kim, M., Pan, S., Neuhierl, B., Perot, F., and Ocampo, J., "Towards engine-mounted exhaust and muffler aeroacoustics predictions using a Lattice Boltzmann based method," FISITA World Congress 2016, F2016-NVHG-027, 2016 .
4. Powell, R., Hendriana, D., Gutzeit, B., Golsch, K. and Fadler, J., "Direct Aeroacoustic Simulation of Flow Impingement Noise in an Exhaust Opening," [J] *SAE Int. J. Passeng. Cars - Mech. Syst.* 4(2):961-969, 2011, doi:10.4271/2011-01-1517.
5. Rose, T., Krüger, J., and Neuhierl, B., "Strömungsakustische Simulation von Abgasanlagen," Magdeburger Symposium für Motor- und Aggregate-Akustik, 2014.
6. Neuhierl, B., "Simulation of Flow-Induced Noise in Exhaust Silencers," Internoise, 2016.
7. Frisch, U., Hasslacher, B., and Pomeau, Y., "Lattice-gas Automata for the Navier-Stokes Equations," *Phys. Rev. Lett.* 56:1505-1508, 1986.
8. Chen, H., Chen, S., and Matthaeus, W., "Recovery of the Navier-Stokes equations using a lattice-gas Boltzmann method," *Phys.Rev. A* 45:5339-5342, 1992.
9. Chen, H., Teixeira, C. and Molvig, K., "Digital physics approach to computational fluid dynamics: Some basic theoretical features" [J], *Intl. J. Mod. Phys. C* 9 (8), 675 (1997).
10. Chen, H., Teixeira, C. and Molvig, K., "Realization of Fluid Boundary Conditions via Discrete Boltzmann Dynamics" [J], *Intl J. Mod. Phys. C*, Vol. 9 (8), pp. 1281-1292, 1998.
11. Thantanapally, C., Singh, S., Succi, S., and Ansumali, S., "Quasi-equilibrium lattice Boltzmann models with tunable Prandtl number for incompressible hydrodynamics" [J], *International Journal of Modern Physics C* 24 (12), 1340004 (2013).
12. Chen, H., "Volumetric Formulation of the Lattice Boltzmann Method for Fluid Dynamics: Basic Concept" [J], *Phys. Rev. E*, Vol. 58, pp. 3955-3963, 1998.
13. Shan, X. and Chen, H., "A general multiple-relaxation-time Boltzmann collision model" [J], *International Journal of Modern Physics C* 18, 635 (2007).
14. Chen, H., Goldhirsh, I. and Orszag, S., "Discrete rotational symmetry, moment isotropy, and higher order lattice Boltzmann models" [J], *J. Sci. Computing*, submitted (August. 2007).
15. Bhatnagar, P., Gross, E. and Krook, M., 1954, "A model for collision processes in gases. I. small amplitude processes in charged and neutral one-component system" [J], *Pys. Rev.*, vol.94, pp.511-525, 1954.
16. Chapman, S. and Cowling, T., "*The Mathematical Theory of Non-Uniform Gases*" [J], Cambridge University Press, 1990.
17. Yakhot, V., "Extended Boltzmann Kinetic Equation for Turbulent Flows" [J], *Science*, Vol. 301, pp. 633-636, 2003.
18. Shan, X. and Chen, H., 1993, "Lattice Boltzmann model for simulating flows with multiple phases and components" [J], *Phys. Rev. E*, 47, 1815-1819.
19. Li, Y., Shock, R., Zhang, R., and Chen, H., 2004, "Numerical Study of Flow Past an Impulsively Started Cylinder by Lattice Boltzmann Method" [J], *J. Fluid Mech.*, Vol. 519, pp. 273-300.

20. Chen, H., Kandasamy, S., Orszag, S., Shock, R., Succi, S. and Yakhot, V., "Extended Boltzmann Kinetic Equation for Turbulent Flows" [J], *Science*, Vol. 301, pp. 633-636, 2003.
21. Chen, H., Orszag, S., Staroselsky, I. and Succi, S., 2004, "Expanded Analogy between Boltzmann Kinetic Theory of Fluid and Turbulence" [J], *J. Fluid Mech*., Vol. 519, pp. 307-314.
22. Zhang, R., Fan, H., and Chen, H. "A lattice Boltzmann approach for solving scalar transport equations." [J], *Philosophical Transactions of the Royal Society A: Mathematical, Physical and Engineering Sciences*, 369(1944), 2264-2273, 2011.
23. Gaylard, A., "CFD Simulation of Side Glass Surface Noise Spectra for a Bluff SUV," *SAE 2006-01-0137*, 2006, doi:10.4271/2006-01-0137.
24. Oettle, N., Meskine, M., Senthooran, S., Bissell, A. et al., "A Computational Approach to Assess Buffeting and Broadband Noise Generated by a Vehicle Sunroof," *SAE Int. J. Passeng. Cars - Mech. Syst.* 8(1):196-204, 2015, 2015, doi:10.4271/2015-01-1532.
25. Pérot, F., Meskine, M., and Vergne, S., "HVAC noise predictions using a Lattice Boltzmann Method," 19th AIAA/CEAS Aeroacoustics conference, May 2013, Berlin, Germany, 2013.
26. Aissaoui, A., Tupake, R., Bijwe, V., Meskine, M, Perot, F., Belanger, A., and Vaidya, R. J., "Flow-Induced Noise Optimization of SUV HVAC System using a Lattice Boltzmann Method" [J], *SAE Int. J. Passeng. Cars - Mech. Syst.* 8(3):1053-1062, 2015, doi:10.4271/2015-01-2323.
27. Laffite, A., and Pérot, F., "Investigation of the Noise Generated by Cylinder Flows Using a Direct Lattice-Boltzmann Approach," AIAA 2009-3268, 13th AIAA/CEAS aeroacoustics conference, Miami, Florida, 2009.
28. Brès, G.A., Pérot, F., and Freed, D., "Properties of the Lattice-Boltzmann Method for Acoustics," AIAA 2009-3395, 13th AIAA/CEAS aeroacoustics conference, Miami, Florida, 2009.
29. Keating, A., Dethioux, P., Satti, R., Noelting, S., Louis, J., Van de Ven, T., and Vieito, R., "Computational Aeroacoustics Validation and Analysis of a Nose Landing Gear," AIAA 2009-3154, 13th AIAA/CEAS aeroacoustics conference, Miami, FL, 2009.
30. Mann, A., Pérot, F., Kim, M.S., Casalino, D., and Fares, E., "Advanced Noise Control Fan Direct Aeroacoustics Predictions using a Lattice-Boltzmann Method," AIAA paper 2012-2287, 16th AIAA/CEAS aeroacoustics conference, Colorado Springs, June 2012, 2012.
31. Balasubramanian, G., Mutnuri, L.A.R., Sugiyama, Z., Senthooran, S., and Freed, D., "A Computational Process for Early Stage Assessment of Automotive Buffeting and Wind Noise," *SAE International Paper 2013-01-1929*, 2013, doi:10.4271/2013-01-1929.
32. Iman, R.L.; Davenport, J.M.; Zeigler, D.K. (1980). *Latin hypercube sampling (program user's guide).*
33. Cressie, N.A.C., "The Origins of Kriging," *Mathematical Geology* 22:239-252, 1990.
34. Sun, S., Chang, Y.-P., Fu, Q., Zhao, J. et al., "Aerodynamic shape optimization of an SUV in early development stage using a response surface method," *SAE Intl. J. Passeng. Cars-Mech. Syst.* 7(4):1252-1263, 2014, doi:10.4271/2014-01-2445.

Contact Information

For further information, please contact **Adrien Mann** at 150 North Hill Dr Ste 30, Brisbane
CA 94005, USA
or via email at amann@exa.com

Or

Clément Nardari
at Landshuter Allee 8 D-80637 München, Germany
or via email at cnardari@exa.com

Definitions/Abbreviations

LBM - Lattice Based Method

SPL - Sound Pressure Levels

OASPL - Overall Sound Pressure Levels

CFD - Computational Flow Dynamics

CAA - Computational-AeroAcoustics

CAD - Computer-Aided Design

ISSN 0148-7191